GV1001 reduces neurodegeneration and prolongs lifespan in 3xTg-AD mouse model through anti-aging effects

Hyun-Hee Park[1,*], Hyuk Sung Kwon[1,*], Kyu-Yong Lee[1,*], Ye Eun Kim[1], Jeong-Woo Son[1], Na-Young Choi[1], Myung-Hoon Han[3], Dong Woo Park[4], Sangjae Kim[5], Seong-Ho Koh[1,2]

[1]Department of Neurology, Hanyang University Guri Hospital, Gyeongchun-ro, Guri-si, Gyeonggi-do 11923, Korea
[2]Department of Translational Medicine, Hanyang University Graduate School of Biomedical Science and Engineering, Seoul 04763, Korea
[3]Department of Neurosurgery, Hanyang University Guri Hospital, Gyeongchun-ro, Guri-si, Gyeonggi-do 11923, Korea
[4]Department of Radiology, Hanyang University Guri Hospital, Gyeongchun-ro, Guri-si, Gyeonggi-do 11923, Korea
[5]Teloid Inc., Los Angeles, CA 90010, USA
*Equal contribution

ABSTRACT

GV1001, which mimics the activity of human telomerase reverse transcriptase, protects neural cells from amyloid beta (Aβ) toxicity and other stressors through extra-telomeric function, as noted in our prior *in vitro* studies. As per a recent phase II clinical trial, it improves cognitive function in patients with moderate to severe dementia. However, the underlying protective mechanisms remain unclear. This study aimed to investigate the effects of GV1001 on neurodegeneration, senescence, and survival in triple transgenic Alzheimer's disease (3xTg-AD) mice. GV1001 (1 mg/kg) was subcutaneously injected into old 3xTg-AD mice thrice a week until the endpoint for sacrifice, and survival was analysed. Magnetic resonance imaging (MRI) and Prussian blue staining (PBS) were performed to evaluate entry of GV1001 entrance into the brain. Diverse molecular studies were performed to investigate the effect of GV1001 on neurodegeneration and cellular senescence in AD model mice, with a particular focus on BACE, amyloid beta$_{1-42}$ (Aβ$_{1-42}$), phosphorylated tau, volume of dentate gyrus, β-galactosidase positive cells, telomere length, telomerase activity, and ageing-associated proteins. GV1001 crossed the blood-brain barrier, as confirmed by assessing the status of ferrocenecarboxylic acid-conjugated GV1001 using magnetic resonance imaging and PBS. GV1001 increased the survival of 3xTg-AD mice. It decreased BACE and Aβ$_{1-42}$ levels, neurodegeneration (i.e., reduced CA1, CA3 and dentate gyrus volume, decreased levels of senescence-associated β-galactosidase positive cells, and increased telomere length and telomerase activity), and levels of ageing-associated proteins. We suggest that GV1001 exerts anti-ageing effects in 3xTg-AD mice by reducing neurodegeneration and senescence, which contributes to improved survival.

INTRODUCTION

Alzheimer's disease (AD) is one of the most critical neurodegenerative disorders, as elderly people over 65 years of age are increasing worldwide [1–3]. AD is a major burden for aging societies worldwide, and its treatment should be established as soon as possible for the future of humans. Although there have been many

studies on the development of AD treatment, there is no definitive cure, except for symptomatic treatment with donepezil, rivastigmine, galantamine, and memantine. Antibodies against amyloid beta (Aβ) have been under clinical trials and have given us hope [4, 5]. For example, aducanumab was approved by the Food and Drug Administration in the United States in June 2021, although its efficacy remains controversial. Despite the use of various antibodies to treat AD, there are still many unmet medical needs.

Aging is an inevitable and definite risk factor for AD, which may accelerate aging [6]. Aging, which is eventually associated with progressive physical deterioration and increased vulnerability to death, cannot be avoided [7]. In contrast to chronological aging, physical aging, which is more important for health and aging-related disorders, may differ between individuals. Physical aging results in processes such as genomic instability, telomere attrition, epigenetic alterations, loss of proteostasis, mitochondrial dysfunction, cellular senescence, deregulated nutrient sensing, stem cell exhaustion, and altered intercellular communication [8], and vice versa. The aging process can increase the activity of β-site amyloid precursor protein cleaving enzyme (β-secretase, BACE), which contributes to the amyloidogenic pathogenesis of AD, and can cause the loss of neurons and synapses in the cerebral cortex, which are the main characteristics of AD [9–11]. Telomere shortening due to aging has also been reported to be closely related to cognitive decline and AD [12, 13]. Due to the importance of the aging process in the pathogenesis of AD [6], anti-aging therapy has been regarded as a possible and valuable treatment for AD. Although there have been many clinical trials using drugs with anti-aging effects for AD, none have shown clinical efficacy and have been approved for clinical use. However, as anti-aging is still considered one of the most fascinating treatments for AD, notable effort has been dedicated to the development of new therapeutic strategies with anti-aging effects.

GV1001 is a small peptide containing 16 amino acids that mimics a fragment of the active catalytic site of human telomerase reverse transcriptase (hTERT). GV1001 has been previously reported to have various biological functions, including antioxidant, anti-inflammatory, anti-aging, anti-apoptotic, and mitochondrial stabilisation effects, mimicking the extra-telomeric function of hTERT [14–16]. Based on these beneficial effects, GV1001 was applied in a phase II clinical trial for the treatment of moderate to severe AD, and the results showed that a significant improvement in cognitive function was observed in patients with moderate to severe AD treated with

GV1001, at weeks 12 and 24 [17]. Despite these beneficial effects of GV1001 in an *in vitro* model of AD and in patients with moderate to severe dementia, the exact *in vivo* mechanisms of action are unclear.

Therefore, we hypothesised that GV1001 might have anti-aging effects and improve neurodegeneration and senescence *in vivo* as a possible mechanism for its beneficial effects on AD. To test these hypotheses, we conducted this study to determine whether GV1001 could increase the survival of triple transgenic Alzheimer's disease (3xTg-AD) mice. In addition, various molecular experiments to analyse the level of BACE, level of amyloid beta$_{1-42}$ (Aβ_{1-42}), volume of the hippocampus and cortex, abundance of senescence-associated β-galactosidase-positive cells, telomere length, telomerase activity, and levels of aging-associated proteins were performed to demonstrate the anti-aging effects of GV1001 on neurodegeneration and senescence in 3xTg-AD mice.

RESULTS

GV1001 enters the brain through the blood-brain barrier (BBB)

To confirm that GV1001 can enter the brain through the BBB, 200 µl of 1 mM ferrocenecarboxylic acid-conjugated GV1001 (Fe-GV1001), which has been verified to enter diverse stem cells very efficiently and can be used to track transplanted stem cells in the brain [18], was injected into the tail vein of 3xTg-AD (B6:129-Psen1tm1Mpm Tg [APPSwe, tauP301L] 1Lfa/Mmjax) and WT mice. Before and after injection, MRI was performed as previously described. MR images showed dots with low signal intensity in the brains (surrounded by yellow circles) of 3xTg AD mice (Figure 1A) and WT mice (Figure 1B) after injection (+ in the figures) compared to before it (- in the figures). These dots were confirmed to be Fe-GV1001 via Prussian blue staining (Figure 1C), and these findings showed that Fe-GV1001 entered the brain across the BBB.

GV1001 significantly improves the survival of old-aged 3xTg AD mice

Survival after starting GV1001 treatment at 21 months was evaluated until the endpoint (Figure 2A), which was determined based on the criteria for an appropriate end-point according to the CCAC guidelines (Supplementary Tables 1, 2), to assess the effect of GV1001 on the life-span of old-aged 3xTg AD mice corresponding to advanced AD [19]. Survival probability analysis showed that GV1001 treatment markedly improved the survival of old-aged 3x Tg AD mice ($p = 0.009$, Figure 2B).

GV1001 reduces Aβ₁₋₄₂ by decreasing BACE and phosphorylated tau (p-tau) in old-aged 3xTg AD mice

Diverse molecular studies have been performed to explain the positive effects of GV1001 on the survival of old-aged 3xTg AD mice. The effect of GV1001 on $A\beta_{1-42}$ expression was investigated using immunohistochemistry (Figure 3A). Treatment with 1 mg/kg of GV1001 noticeably diminished the expression of $A\beta_{1-42}$ in the brains of 3xTg AD mice compared with that of saline-treated mice (Figure 3A and Supplementary Figure 1A). BACE is a key enzyme in $A\beta_{1-42}$ production; therefore, the expression of BACE was also evaluated using western blotting and immunohistochemistry. The results showed that 1 mg/kg of GV1001 significantly decreased BACE expression (Figure 3B, 3C). To double-check the effect of GV1001 on BACE expression, NSCs were treated with 20 µM $A\beta_{25-35}$ and/or different doses of GV1001 (1 and 10 µM) *in vitro*, and BACE expression was considerably reduced in NSCs treated with GV1001 (Figure 3D). In addition, treatment with 1 mg/kg of
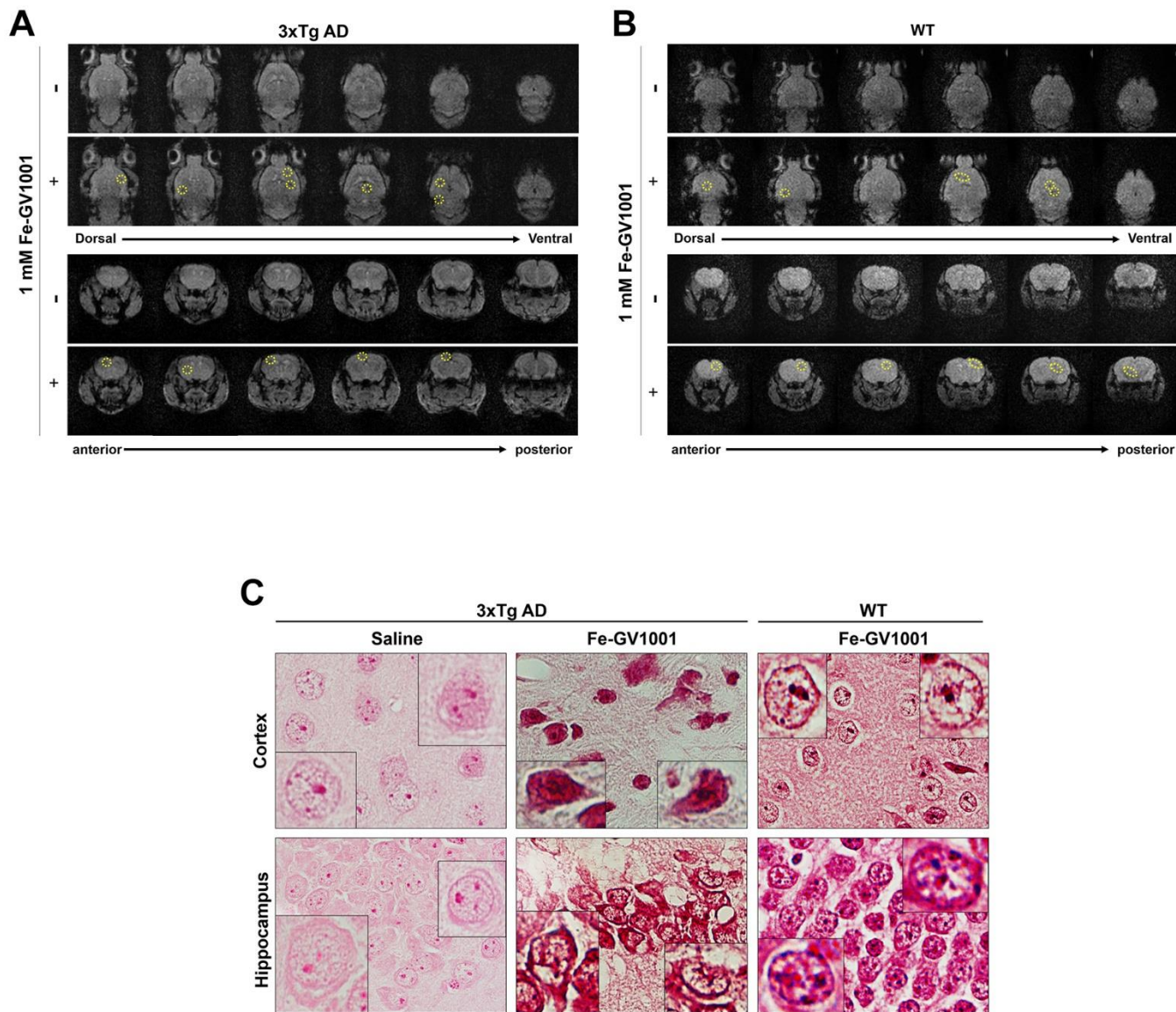

Figure 1. Penetrance of GV1001 into the brain through the blood-brain barrier. (**A**, **B**) We performed magnetic resonance imaging (MRI) to determine whether GV1001 could enter the brain. Ferrocenecarboxylic acid (Fe)-GV1001 (1 mg/kg) was subcutaneously injected into 3xTg-AD (12-month-old) and wild-type (WT) (8-month-old) mice. After 1 h, two-dimensional (2D) axial (Axl) fast field echo (FFE) and 2D coronal (Cor) FFE images were acquired using 3 T MRI. The entire brain was observed in several sections in the dorsoventral and anteroposterior planes using 2D Axl FFE and 2D Cor FFE images. This result shows that GV1001, represented by dark signals, entered the brains of both 3xTg-AD and WT mice (yellow circles in A and B, respectively). (**C**) Prussian blue staining.

GV1001 reduced the expression of p-tau (S202. T205) in the hippocampus of 3xTg AD mice (Figure 3E and Supplementary Figure 1B).

GV1001 markedly inhibited neurodegeneration and senescence of the hippocampus in old-aged 3xTg AD mice

Nissl staining showed that neurodegeneration of the hippocampus was dominant in old-aged 3xTg AD mice, but treatment with 1 mg/kg of GV1001 markedly inhibited neurodegeneration (Figure 4A). The same finding was also found in immunohistochemistry using an anti-NeuN antibody specific for neurons (Figure 4B). Western blotting of the hippocampus of old-aged 3xTg AD mice showed that treatment with 1 mg/kg of GV1001 extensively increased the expression of NeuN and Tuj1, which are neuronal markers (Figure 4C), which is consistent with the results of nissl staining and IHC.
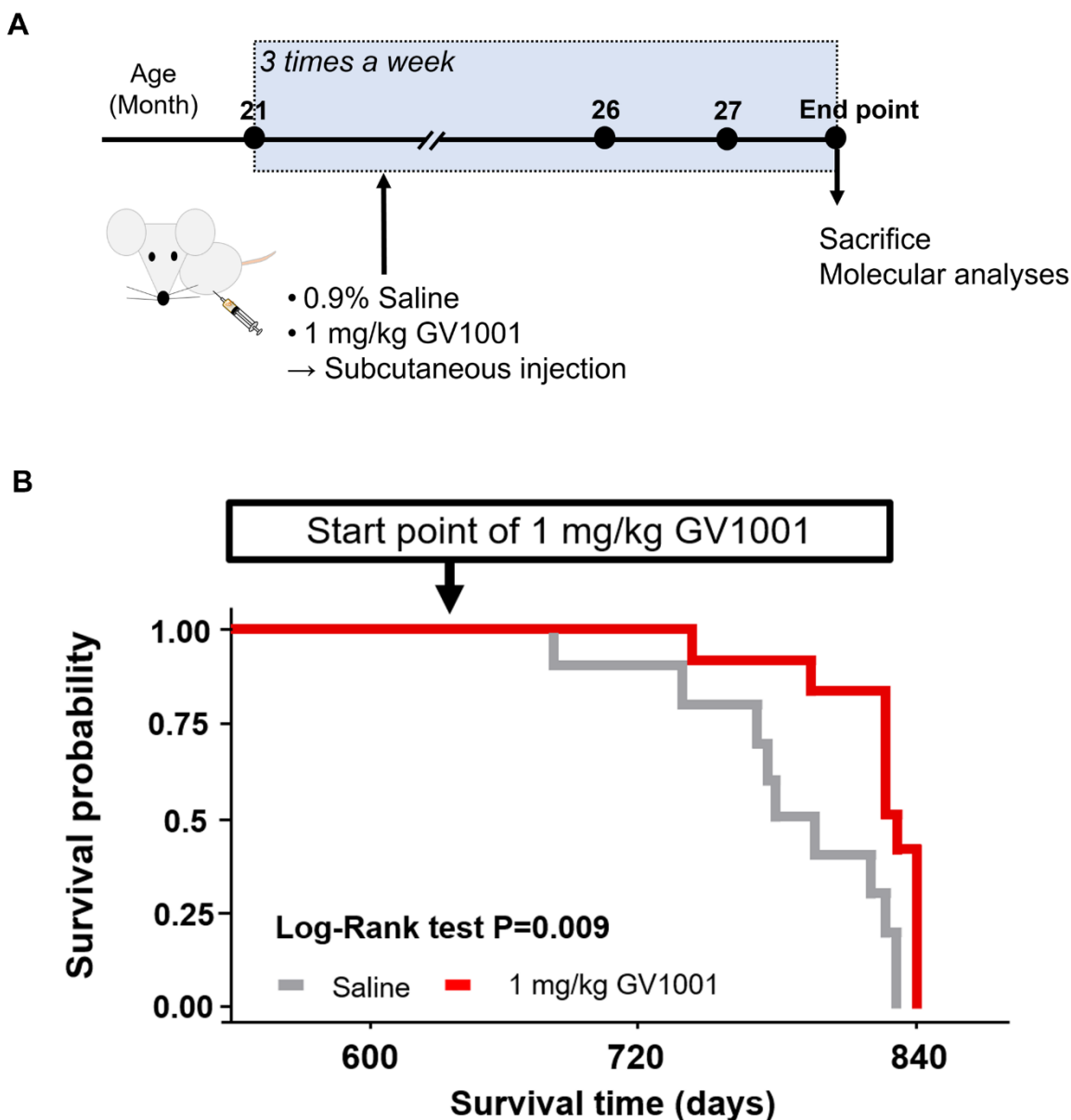

Figure 2. Survival of old 3xTg-AD mice after GV1001 treatment. (**A**) 1 mg/kg of GV1001 or an equivalent volume of 0.9% saline was subcutaneously injected into old-aged 3xTg-AD mice (n = 10 [male =5 and female 5]; control, n = 12 [male = 7 and female = 5]; 1 mg/kg of GV1001) from the age of 21 months until the mice were considered ready to sacrifice (endpoint). Injections were administered thrice a week until the endpoint. (**B**) Survival curves plotted using the Kaplan-Meier estimator. The survival of mice was markedly prolonged by administration of 1 mg/kg.

Effect of GV1001 against neurodegeneration and senescence in the brain of old-aged 3xTg AD mice was achieved through anti-senescence activity

Markers used to predict cell senescence, such as SA-β-Gal, telomerase activity, telomere length, p53, p16^Ink4a, IL-6, and HMGB1, were measured in the brains of old-aged 3xTg AD mice. The results showed that SA-β Gal-positive cells were significantly reduced by treatment with 1 mg/kg GV1001 compared to saline treatment (Figure 5A). Telomerase activity, which is essential to maintain telomere length, and telomere length, which is well known to decrease with senescence of cells, were improved in the brains of old-aged 3xTg AD mice treated with 1 mg/kg of GV1001 (Figure 5B, 5C).

Intracellular markers of senescence, such as p53, p16^{Ink4a}, IL-6, and HMGB1, were considerably decreased in the brains of old-aged 3xTg AD mice treated with 1 mg/kg of GV1001 (Figure 5D). These results suggest that the effect of GV1001 on neuro-degeneration in the brains of old-aged 3xTg AD mice may be related to its anti-senescence activity.

Bioinformatics using the results of proteomics and RNA sequencing also suggests that GV1001 has the anti-senescence effect

A messenger ribonucleic acid (mRNA) sequencing was performed to evaluate the effect of GV1001 on the expression of mRNAs in the brains of 3xTg AD mice,
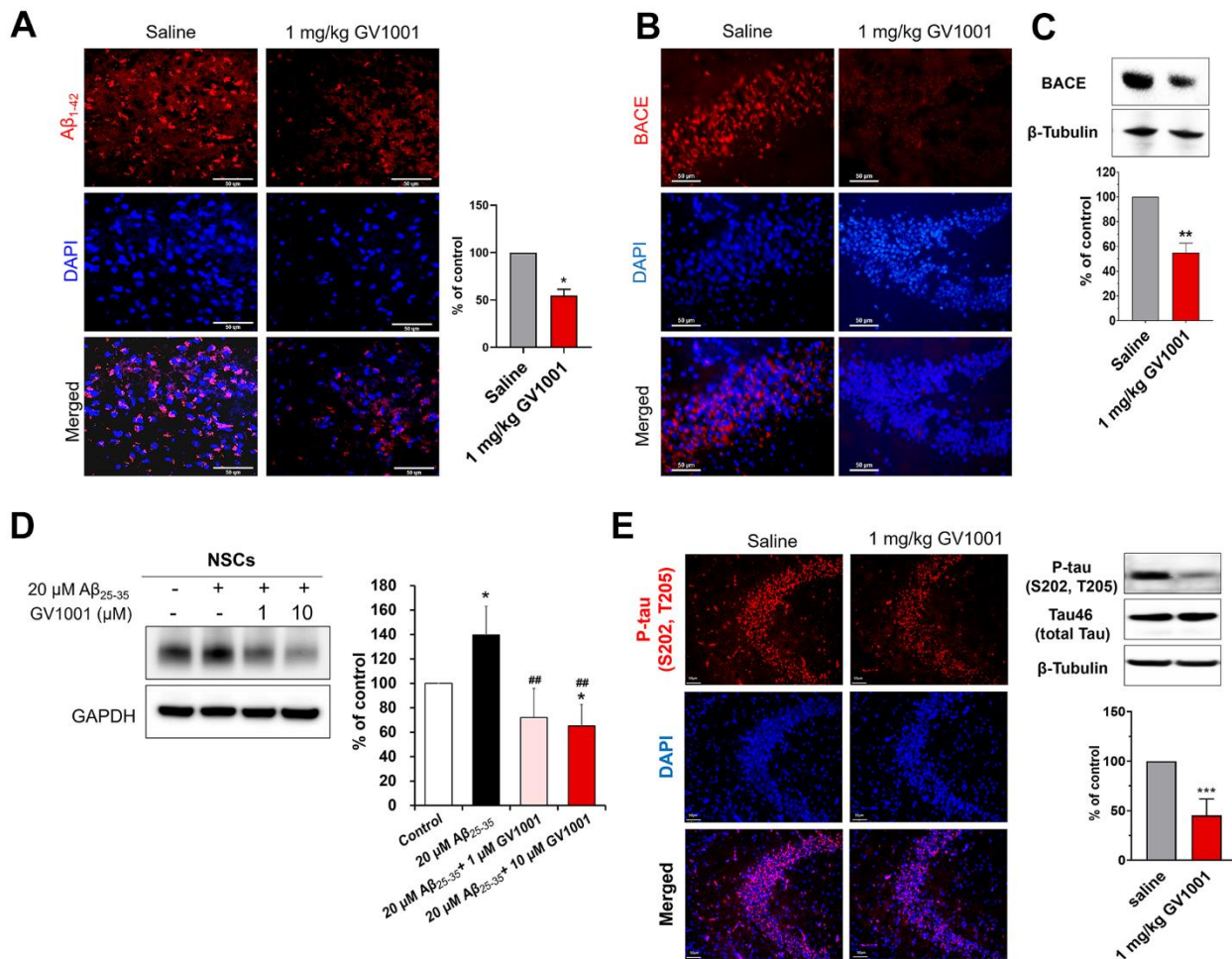

Figure 3. Effect of GV1001 on amyloid beta, β-secretase (BACE) and p-tau levels. (**A**) GV1001 significantly ameliorated the levels of Aβ$_{1-42}$ in the brains of aged 3xTg-AD mice. (**B**, **C**) Expression of BACE was downregulated in old 3xTg-AD mice after treatment with 1 mg/kg GV1001, as shown by western blotting (**B**) and immunohistochemistry (**C**). (**D**) NSCs were isolated from embryonic rodent brains, cultured, and expanded. Then, they were treated with different concentrations of GV1001 (0, 1, or 10 μM) and 20 μM Aβ$_{25-35}$ for 48 h. The expression of BACE was markedly upregulated in NSCs following treatment with 20 μM Aβ$_{25-35}$, although treatment with 1 or 10 μM GV1001 significantly downregulated the expression of BACE. (**E**) GV1001 significantly reduced the levels of p-tau in the hippocampus (CA3). Data are expressed as the mean (% of control) ± standard deviation of three to five independent experiments. The treatment groups were compared using Tukey's post-hoc test after one-way or two-way ANOVA. *$p < 0.05$; **$p < 0.01$ (vs. the control group), ##$p < 0.01$ (vs. NSCs treated only with 20 μM Aβ). Scale bar = 50 μm.

and the results were analysed using ClueGO. The significant functional enrichment results of the upregulated and downregulated mRNAs after GV1001 treatment were visualised using ClueGO (Figure 6A). An interesting finding of the GO analysis was the detection of critical pathways and functions, such as the regulation of cellular senescence, p53 signalling, positive regulation of telomere maintenance through telomere lengthening, long-term memory, positive regulation of cAMP biosynthesis, and aging. ClueGO analysis showed that GV1001 strongly affected the levels of senescence-related mRNAs.

Proteomics also confirmed that this effect of GV1001 in the brains of 3xTg AD mice was achieved through diverse intracellular signalling pathways (Figure 6B–6D). The heat map shows protein levels (Figure 6B). Protein expression values were log2-transformed. Red indicates

a high expression level, and green indicates a low expression level (Figure 6C). The survival-related proteins including prohibitin [20, 21], dihyropyridinase-realated protein 2 (DPYSL2) [22], transketolase [23], pyruvate kinase isoform M2 (PKM2) [24], spectrin alpha 2 (spna2) [25] and aconitate hydratase [26] were increased with GV1001 treatment. STRING analysis showed up- and downregulated protein–protein interaction networks. Upregulated and downregulated proteins were clustered based on the STRING evidence score (Figure 6D).

DISCUSSION

In the present study, we confirmed that GV1001 well enters the brain crossing the blood-brain barrier (Figure 1) and significantly prolongs the lifespan of AD transgenic mice (Figure 2) through diverse antiaging effects. As detailed evidence on GV1001's anti-aging
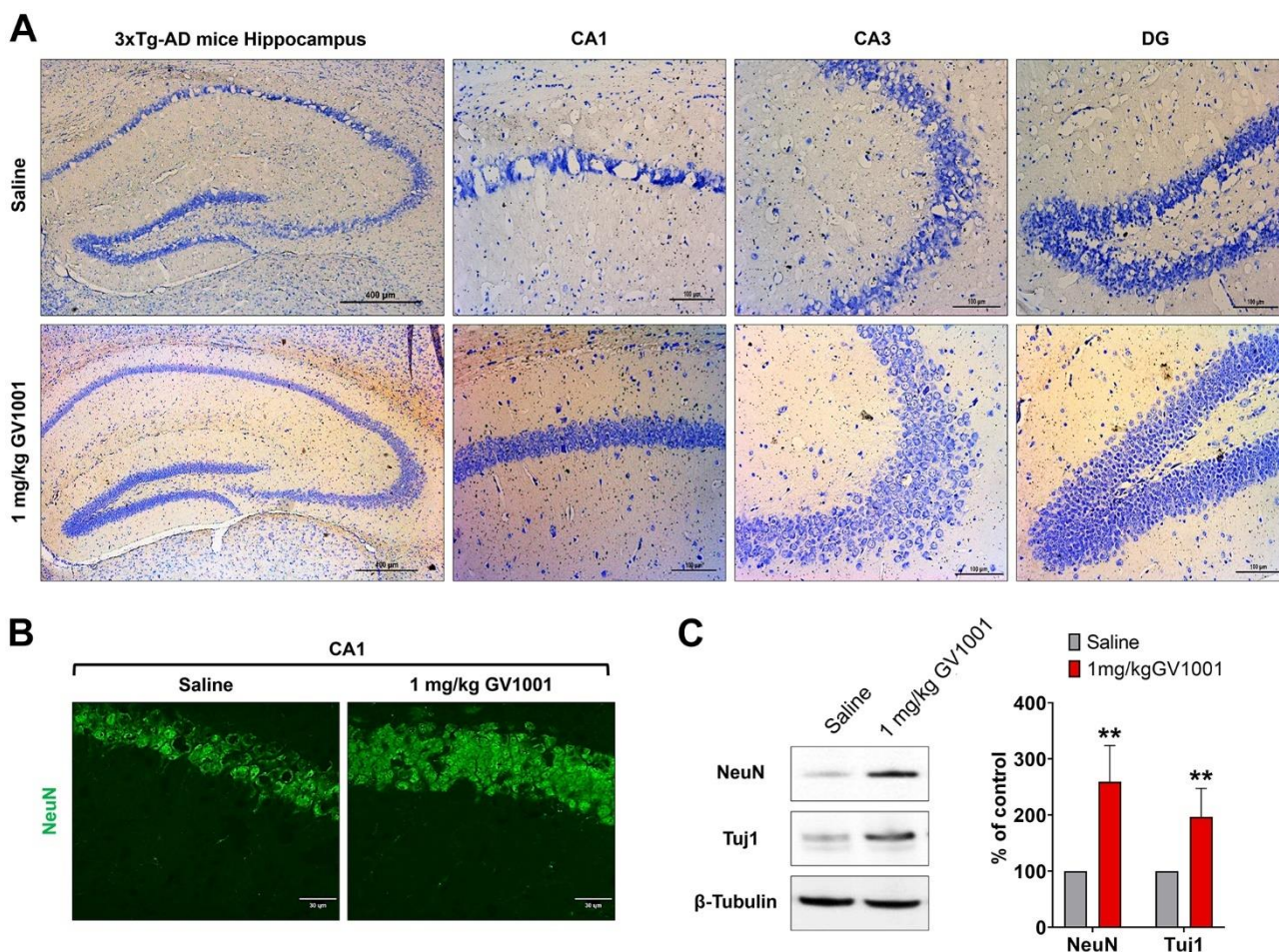

Figure 4. Effect of GV1001 on neurodegeneration. Markers of neurodegeneration were studied in aged 3xTg-AD mice treated with GV1001 and saline. (**A**) Neurodegeneration was evaluated by the volume of the CA1, CA3 and dentate gyrus (DG) in the hippocampus and (**B**, **C**) expression of neuronal markers, such as neuronal nuclei (NeuN) and neuron-specific β III tubulin (Tuj1) of the CA1 in the hippocampus. GV1001 markedly prevented neuronal loss in the hippocampus of 3xTg-AD mice. *$P < 0.05$; **$P < 0.01$ (vs. the control group). Scale bar = 30 μm (a) and 100 μm (b).

effects, GV1001 reduced levels of $A\beta_{1-42}$ (Figure 3A) and BACE (β-secretase) (Figure 3B–3D) and it also restored volume of CA1, CA3 and dentate gyrus and increased neuronal markers in the hippocampus (Figure 4). Senescence-associated β-galactosidase positive cells and intracellular signaling proteins associated with aging were markedly decreased with GV1001 treatment (Figure 5A). In addition, GV1001 enhanced telomerase activity (Figure 5B) and increased telomere length (Figure 5C). RNA-seq and proteomics also confirmed that GV1001 inhibited aging-related signaling pathways and boosted anti-aging-associated ones (Figure 6).
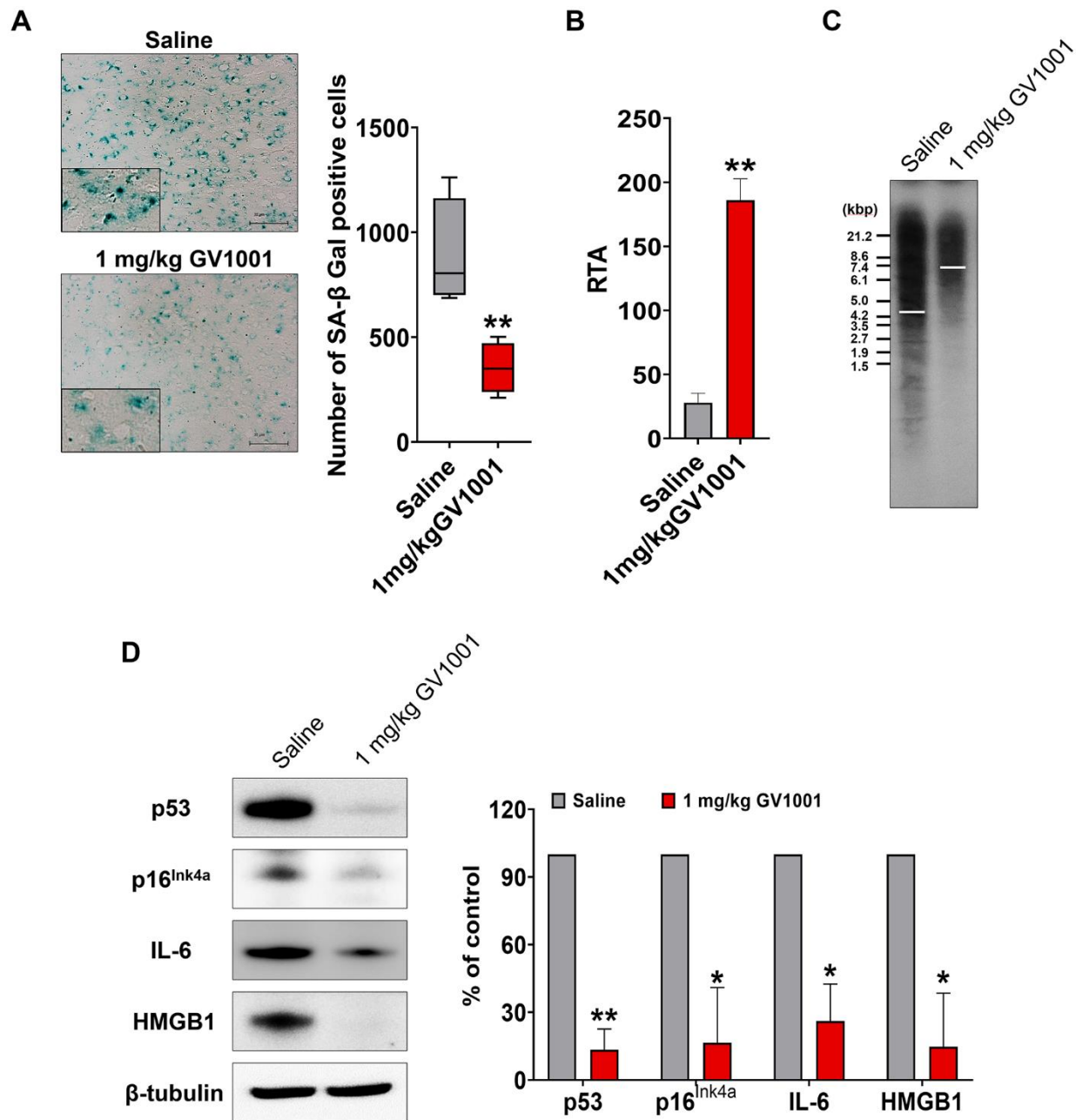

Figure 5. Effect of GV1001 on senescence. Markers of senescence were studied in middle-aged and old 3xTg-AD mice treated with GV1001 or saline. (**A**) GV1001 markedly reduced the expression of senescence-associated β-galactosidase, a well-known senescence marker, in old-aged 3xTg-AD mice. (**B**, **C**) Telomerase activity and telomere length were evaluated as senescence markers. GV1001 significantly increased both parameters in old-aged 3xTg-AD mice (B and C, respectively). (**D**) The expression of senescence markers, such as p53, p16[Ink4a], interleukin-6, and high mobility group protein B1, in the brains of old 3xTg-AD mice treated with GV1001 and saline, was assessed, and the results showed that the expression levels of all senescence markers decreased in old-aged 3xTg-AD mice after treatment with GV1001. *$P < 0.05$; **$P < 0.01$ (vs. the control group). Scale bar = 30 μm (a, b).
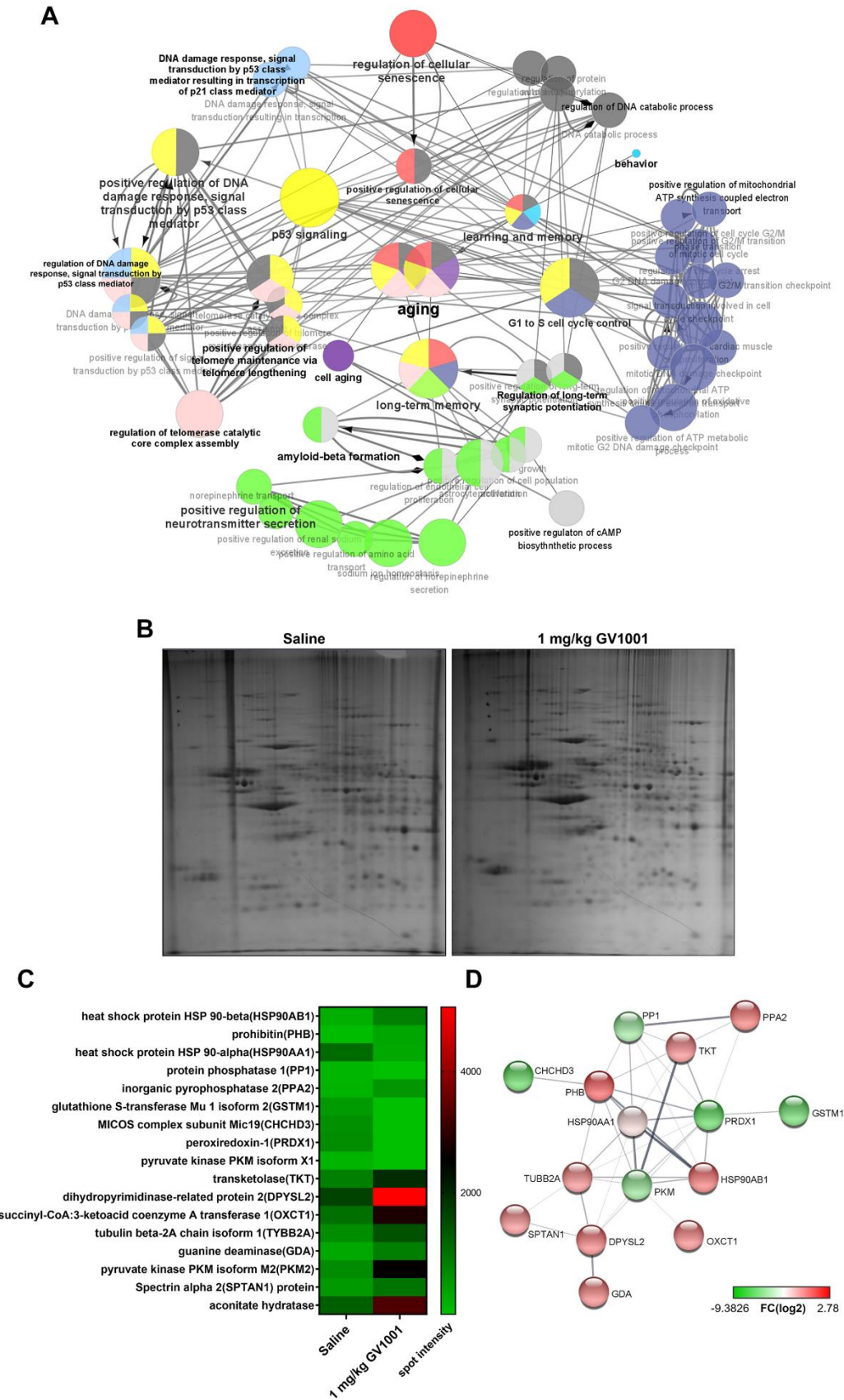
Figure 6. Effect of GV1001 on aging, telomere maintenance, and long-term memory confirmed via bioinformatics analysis. (**A**) ClueGO analysis visualised the significant functional enrichment results of upregulated and downregulated mRNAs associated with

inflammation in old-aged 3xTg-AD mice treated with GV1001 compared to those treated with saline, using the Gene Ontology (GO) functional network. mRNAs that show significant differential expression are selected for analyses based on the following criteria: more than three-fold change, normalised data (log2) >4, and p < 0.05. The functionally grouped networks of the gene regulatory network and the target genes of these hub nodes were transferred to ClueGO and grouped as functional clusters. All nodes have been linked based on their kappa scores (≥0.3). Only the most significant term per group is labelled in bold, and their colours represent the functional groups to which they belong. Node size represents enrichment significance. (**B**) Proteomics show that GV1001 affected the levels of various intracellular proteins in the brains of 3xTg AD mice. Two-dimensional (2D) gel electrophoresis images. The first dimension is run using a 13-cm IPG strip with a pH gradient from 4 to 10. Coomassie blue staining is used to identify 24 proteins that increased or decreased more than two-fold. (**C**) Heat map shows protein levels. Protein expression values are log2-transformed. Red indicates a high expression level; green indicates a low expression level. (**D**) STRING analysis (functional protein association networks database, http://string-db.org/) of upgregulated and downregulated proteins. Proteins are clustered based on the STRING evidence score. PPA2, inorganic pyrophosphatase 1; GSTM1, glutathione S-transferase Mu 1 isoform 2; MICOS, mitochondrial contact site and cristae organising system; CHCHD3, complex subunit Mic19; PRDX1, peroxiredoxin-1; DPYSL2, dihydropyrimidinase-related protein 2; OXCT1, succinyl-CoA:3-ketoacid coenzyme A transferase 1; TYBB2A, tubulin beta-2A chain isoform 1; SPTAN1, spectrin alpha 2; PHB, prohibitin; TKT, transketolaseHSP90AA1, HSP90AA1, heat shock protein 90 alpha class A member 1; HSP90AB1, heat shock protein 90 alpha class B member 1.

Aging is an undeniable risk factor for AD and it leads to many changes like genomic instability, telomere attrition, epigenetic alterations, loss of proteostasis, mitochondrial dysfunction, cellular senescence, deregulated nutrient sensing, stem cell exhaustion, and altered intercellular communication [8], all of which are also well-established pathomechanism of AD. It is well known that level of BACE and senescence-associated β-galactosidase positive cells increases [10, 27] and telomere length and telomerase activity decreases [28] with aging. These are also related to the progression of AD. BACE and Aβ$_{1-42}$ are related to amyloidogenic process after processing amyloid precursor protein (APP) [11]. Reducing the level of BACE and Aβ$_{1-42}$ by GV1001 in 3xTg-AD mice, found in this study, indicates the possibility of GV1001 to cut down on amyloidogenic pathogenesis of AD by ameliorating initiation of Aβ formation.

Senescence-associated β-galactosidase positive cells and telomere attrition are well-known biomarkers for aging [27, 29]. Increased activity of β-galactosidase, which suggests the accelerated aging, is also found in AD [30]. Telomere length, a predictor of the future life of cells, progressively shortens with each cell division and aging process and it can be reversed by the telomerase [28, 31]. Telomerase is known to maintain telomere structure and decreased telomerase activity affects telomere shortening and cellular senescence [28, 32]. Shortening of telomere can also occur with aging of organism and shorter telomere length is linked to accelerated aging [31, 33]. Both shortening of telomere length and progression of AD have been reported to be associated with oxidative stress and inflammation [34, 35]. Shorter telomere length is known to be correlated with the mortality of general population and the risk of AD [13, 36]. In this study, GV1001 efficiently reduced β-galactosidase-positive cells and senescene-associated proteins and increased telomere length and telomerase activity in 3xTg-AD mice. These results represent GV1001 has anti-aging effects against accelerated aging

in AD mice and can explain the increment of survival of them.

The expression of survival-related proteins, including prohibitin (PHB) [20, 21], dihydropyridinase-related protein 2 (DPYSL2) [22], transketolase (TKT) [23], pyruvate kinase isoform M2 (PKM2) [24], spectrin alpha 2 (SPTAN1) [25], and aconitate hydratase [26], increased with GV1001 treatment. According to proteomics, the levels of survival-related proteins, such as PHB, TKT, DPYSL2, PKM2, SPTAN1, and aconitate hydratase, increased after treatment with GV1001. PHB is known to affect mitochondrial membrane composition and its functionality [20]. Loss of PHB impairs mitochondrial architecture and leads to tau hyperphosphorylation and neurodegeneration [21]. TKT regulates the proliferation of hippocampal progenitor cells, and attenuation of TKT activity inhibits their proliferation [23]. PKM2 is found in the brain and liver and is involved in the repair and regeneration of these tissues [24]. SPTAN1 is a spectrin family protein expressed in neurons and glia and plays a role in stabilising the cytoskeleton [25]. Levels of aconitate hydratase, which is involved in energy generation and antioxidant systems, decrease with age [26, 37]. In conclusion, increasing the levels of the proteins described above might have a protective effect against neurodegeneration. Currently available treatments for AD (acetylcholinesterase inhibitors and N-methyl-D-aspartic acid receptor antagonists) have beneficial effects on cognition, function, behaviour, and clinical global changes in patients with AD [38]. However, they are not considered disease-modifying treatments that alter the underlying pathomechanism of AD [39]. According to a recent randomised controlled clinical trial, treatment with GV1001 improved cognitive function in patients with moderate to severe dementia compared to placebo treatment [17]. In addition to the previously confirmed effects of GV1001 (anti-oxidant, anti-inflammatory, anti-aging, antiapoptotic, and mitochondrial stabilisation effects) [14, 40], the

neuroprotective effect confirmed in the current study (improving survival, reducing BACE and $A\beta_{1-42}$, reducing atrophy of the dentate gyrus, and improving senescence in 3xTg-AD mice) explains the mechanisms of GV1001. GV1001 targets multiple processes of AD and may be a good candidate for disease-modifying treatments for AD.

Considering our previous *in vitro* findings [14, 15, 18], the beneficial effects of GV1001 are suggested to be related to its extra-telomeric function. The extra-telomeric function of hTERT affects various cellular processes, such as metabolism, stress response, epigenetic regulation, and mitochondrial function. Extra-telomeric function contributes to the regulation of chromatin structure, gene expression, DNA damage response, and interaction with various signalling pathways in the nucleus; it controls stress particles under non-stressed conditions, interacts with signalling pathways in the cytoplasm, reduces mitochondrial ROS and apoptosis, protects mitochondrial DNA, improves respiration, and increases complex 1 activity in mitochondria [41, 42]. All these effects on the extra-telomeric function of hTERT coincide with the most important changes during the anti-aging process [43, 44]. A recent study also suggested that increasing TERT with telomerase-increasing compounds protected hippocampal neurons from Aβ toxicity by enhancing the gene expression of neuronal survival and plasticity [39]. Also, GV1001 and gonadotropin-releasing hormone receptors (GnRHRs) were highly colocalized and GV1001 activated downstream of GnRHRs [45]. Beneficial effects of GV1001 were blocked after knockdown of GnRHRs [45]. It is reasonable to believe that the anti-aging effects of GV1001 in 3xTg-AD mice demonstrated in this study are also associated with extra-telomeric function and activating GnRHRs as an important mode of action against AD.

Some limitations of this study must be considered. First, animal models are of familial AD and cannot reflect the heterogeneous nature of humans enrolled in clinical trials [46]. The results of this study cannot explain all protective effects of GV1001. A more diverse protective mechanism of GV1001 in AD, including its anti-inflammatory effects, needs to be confirmed *in vivo*.

In conclusion, accelerated aging and AD are closely related, and this study confirmed that GV1001 has multiple anti-aging effects. These effects, including reducing neurodegeneration, BACE, $A\beta_{1-42}$, atrophy of the dentate gyrus, and senescence, may improve the survival of 3xTg-AD mice and serve as evidence to explain the positive results shown in a clinical trial for the treatment of moderate to severe AD.

MATERIALS AND METHODS

Animals

Every effort was made to minimise the number of animals used and limit animal suffering. Each animal was used once. Old-aged 3xTg-AD mice (B6; 129-Psen1 tm1Mpm Tg [APPSwe, tauP301L] 1Lfa/Mmjax) and corresponding wild-type (WT) (B6129SF2/J) mice used in the experiments were obtained from Jackson Laboratory (Bar Harbour, ME, USA).

In this study, experimental 3xTg-AD mice (21 months old) were divided into two groups, with 12 animals assigned to each group. The experimental groups were as follows: 1) 0.9% saline and 2) 1 mg/kg of GV1001 (the most effective dose confirmed in another middle-aged 3xTg-AD mice study, Supplementary Figures 1, 2). GV1001 or an equivalent volume of saline was subcutaneously injected into old-aged 3xTg-AD mice three times a week from the age of 21 months to the endpoint for sacrifice, identified according to the Canadian Council on Animal Care (CCAC) guidelines (Supplementary Tables 1, 2), in a blinded manner [47]. The survival curves of old-aged 3xTg-AD mice were generated using the Kaplan-Meier method.

Magnetic resonance imaging (MRI)

To visualise GV1001 in the brains of 3xTg-AD and WT mice by MRI, ferrocenecarboxylic acid (Fe) was conjugated to GV1001. Two-dimensional (2D) imaging with axial (Axl) fast field echo (FFE) and 2D coronal (Cor) FFE MRI was performed using a DS Micro 47 coil (Philips, Cambridge, MA, USA) with a 3.0 T MRI device (Philips, 3.0 T Ingenia CX, The Netherlands). Mouse brains were imaged using 2D Axl FFE MRI [repetition time/time echo (TR/TE) = 596 ms/16 ms; number of signal averaging (NSA) = 10 ms; sense = 2; slide thickness/gap = 0.8/0 mm; matrix = 132×130; field of view (FOV) = 39×39 mm] and 2D Cor FFE MRI (TR/TE = 596/16 ms; NSA = 10 ms; sense = 2; slide thickness/gap = 0.7/0 mm; FOV = 39 $\times$ 39 mm) before the injection of GV1001. The 3xTg-AD and WT mice received intravenous injections of 10 mM Fe-GV1001 (diluted, 1:10; volume, 200 μL). After 1 h, 2D Axl FFE and 2D Cor FFE images were obtained. The entire brain was observed in several sections of the dorsoventral and anteroposterior (AP) planes. All animals were sacrificed for histological examination at the end of the MRI.

Prussian blue staining (iron staining)

Brain tissue samples from 3xTg-AD and wild-type mice were fixed in 4% paraformaldehyde, embedded

in paraffin, sectioned (thickness, 3 μm), and transferred to slides. The samples were incubated in ethanol and xylene for 3 min each for deparaffinization and washed three times with deionized water. Thereafter, the slides were incubated in 10 ml iron staining solution (equal volumes of potassium ferrocyanide and hydrochloric acid solution) for 3 min and washed with deionized water. The slides were then incubated in nuclear fast red solution for 5 min, washed with deionized water, and allowed to dry. The slides were then mounted with mounting solution and observed under an ultraviolet light microscope, (Olympus Bx53 microscope, Olympus, Tokyo, Japan).

Immunofluorescence staining

Brain tissues from old (21 months old) and middle-aged (12 months old) 3xTg-AD mice were perfused with 0.9% sodium chloride (NaCl) and 4% paraformaldehyde for fixation. The fixed tissues and cells were sectioned using a cryostat, washed three times in 0.01 M phosphate-buffered saline (PBS), and permeabilised in 50% alcohol for 30 min. They were then incubated in 0.3% H_2O_2 in PBS for 20 min, followed by incubation with 10% foetal bovine serum (FBS; Gibco, Grand Island, NY, USA) in PBS for 60 min. Cells were incubated overnight in 2% normal serum in PBS containing the following primary antibodies: rabbit anti-beta amyloid 1-42 antibody (1:100, ab10148, Abcam, UK), rabbit anti-BACE (1:100, 5606, Cell Signalling, USA) and phospho-Tau (Ser202, Thr205) (1:100; MN1020; Invitrogen, USA), mouse anti-neuronal nuclei (NeuN) (1:100; MAB377, Millipore, USA).

The following day, cells were incubated for 60 min in 2% normal serum in PBS containing the following secondary antibodies: Alexa Fluor 488-conjugated goat anti-rabbit (Molecular Probes, Eugene, OR, USA), tetramethylrhodamine-conjugated anti-rabbit (Molecular Probes), Alexa Fluor 488-conjugated goat anti-rabbit (A11008, Invitrogen), Alexa Fluor 594-conjugated goat anti-rabbit immunoglobulin G (IgG) (H+L) (A11037, Thermo Fisher Scientific, Waltham, MA, USA), Alexa Fluor-594-conjugated cross-adsorbed donkey anti-goat IgG (H+L) (A11058, Invitrogen), and Alexa Fluor 350-conjugated cross-adsorbed donkey anti-goat IgG (H+L) (A21081, Invitrogen). Cells were washed several times with PBS and mounted on glass slides with a mounting medium containing 4′,6-diamidino-2-phenylindole (DAPI) (P36931, Invitrogen). Immunostained cells were observed using a confocal fluorescence microscope (K1-fluo, Nanoscope Systems Inc., Daejeon, Korea; DMIRB, Leica, Wetzlar, Germany) at the appropriate excitation wavelengths.

Neural stem cell culture

Neural stem cells (NSCs) were isolated from embryonic rodent brains, cultured, and expanded. The NSC line was cultured as previously described [48–51]. Briefly, Sprague Dawley rat embryos were decapitated on embryonic day 13 (E13). The brains were rapidly removed and placed in a Petri dish half full of ice-cold Hank's balanced salt solution (137 mM NaCl, 5.4 mM potassium chloride, 0.3 mM sodium phosphate dibasic, 0.4 mM potassium phosphate monobasic, 5.6 mM glucose, and 2.5 mM 4-(2-hydroxyethyl)-1-piperazineethanesulphonic acid; GIBCO BRL). Single cells were dissociated from the whole cerebral cortex, lateral ganglionic eminence, and ventral midbrains of foetal rats. The resulting cells were plated at a density of 2×10^4 cells/cm^2 in culture dishes precoated with poly-L-ornithine/fibronectin in Ca^{2+}/Mg^{2+}-free PBS (Gibco) and cultured in N2 medium (Dulbecco's modified Eagle's medium/nutrients mixture F-12, 25 mg/L insulin, 100 mg/L transferrin, 30 nM selenite, 100 μM putrescine, 20 nM progesterone, 0.2 mM ascorbic acid, 2 nM L-glutamine, 8.6 mM D(+) glucose, and 20 nM sodium bicarbonate; Sigma, St. Louis, MO, USA) supplemented with basic fibroblast growth factor (10 ng/mL; R&D Systems, Minneapolis, MN, USA). The cultures were maintained at 37° C in a humidified 5% CO_2 atmosphere for 4–6 days.

Western blotting

The levels of Aβ$_{1-42}$, BACE, p-tau (phosphorylated at S202 and T205), NeuN, doublecortin (DCX), neuron-specific beta-III tubulin (Tuj1), tumour protein 5 (p53), cyclin-dependent kinase inhibitor 2A (CDKN2A/p16^{INK4a}), interleukin-6 (IL-6), high mobility group box (HMGB1), β-tubulin and Glyceraldehyde-3-Phosphate dehydrogenase (GAPDH) were analysed using western blotting, immediately after treatment for 1 or 8 h and after sacrifice. The tissue and cells were harvested, washed once with ice-cold PBS, and resuspended in 1.0 mL of 1× cytosol extraction buffer mix containing dithiothreitol (DTT) and protease inhibitors. After 10 min of incubation on ice, the cell suspension was sonicated (Sonoplus) five to ten times on ice. The samples were centrifuged at 3,000 rpm and 4° C for 10 min, and the supernatants were centrifuged again at 13,000 rpm for 30 min. Samples containing equal amounts (30 μg) of protein were resolved using 10% sodium dodecyl sulphate-polyacrylamide gel electrophoresis (SDS-PAGE) and transferred to nitrocellulose membranes (Amersham Pharmacia Biotech, Buckinghamshire, UK). The membranes were blocked with 5% skim milk and incubated with specific primary antibodies. The following antibodies were used: anti-beta amyloid 1-42 antibody (1:1000, ab10148, Abcam), anti-BACE

(1:1000, 5% BSA, Cell Signalling), phospho-Tau (Ser202, Thr205) (1:500; MN1020; Invitrogen), anti-NeuN (1:1000, 5% BSA, MAB377, Millipore), anti-DCX (1 µg/mL, 5% BSA, ab28941, Abcam), anti-Tuj1 (1:1000, 5% BSA, ab18207, Abcam), anti-p53 (1:1000, 5% BSA, 2524, Cell Signalling), anti CDKN2A/p16^{INK4a} (1:2000, 5% BSA, ab211542, Abcam), anti-IL-6 (1:20, 5% BSA, ab7737, Abcam), anti-HMGB1 (1:1000, 5% BSA, 3935, Cell Signalling), anti-β-tubulin (1:2000, 5% BSA, 2146, Cell Signalling), and anti-GAPDH (1:1000, 5% BSA, Cell Signalling). The membranes were washed with Tris-buffered saline containing 0.1% Tween-20, processed using horseradish peroxidase (HRP)-conjugated anti-rabbit or anti-mouse secondary antibody (Jackson ImmunoResearch Laboratories, Inc., West Grove, PA, USA), and detected using the enhanced chemiluminescence method (GenDEPOT, Katy, TX, USA). The bands were quantified using an image analyser (ImageQuant LAS 4000, GE Healthcare, Little Chalfont, UK).

Nissl body staining

Slices of the hippocampal CA1, CA3 and dentate gyrus (DG) region of the brains of 3xTg-AD mice were air-dried and soaked overnight in 1:1 alcohol:chloroform. The slices were then immersed in 0.1% cresyl violet solution (0.1 g cresyl violet acetate (c5042, Sigma, St. Louis, MO, USA) and 10 drops of glacial acetic acid (PHR1748, Sigma) for 10 min at 37° C. After incubation, slices were washed with distilled water and soaked in 95% ethyl alcohol for 30 min. Microscopic examination revealed the presence of distinct Nissl bodies. The slices were dehydrated with anhydrous alcohol, cleared in xylene, and mounted on glass slides using a mounting medium (Merck, Kenilworth, NJ, USA). The Nissl bodies were then observed under a Leica microscope (DM4000B, Leica Biosystems) to take 4× and 20× bright field images.

Senescence-associated-β-galactosidase (SA-β-Gal) staining

The SA-β-Gal activity was measured using a β-gal staining kit (9860, Cell Signalling Technology) according to the manufacturer's instructions. Briefly, fixed tissues were washed twice with PBS and stained with a β-gal staining solution containing 5-bromo-4-chloro-3-indolyl-b-D-galactopyranoside. Following overnight incubation at 37° C, blue-stained senescent cells were identified under a confocal fluorescence microscope (K1-Fluo, Nanoscope Systems Inc.).

Telomerase activity

Telomerase activity was measured using the TeloTAGGG Telomerase PCR enzyme-linked immunosorbent assay (ELISA)^{PLUS} kit (Roche Applied Science, Penzberg, Germany) according to the manufacturer's instructions. Cells were fluorimetrically assessed using an ELISA plate reader (Synergy H1 Hybrid Reader, BioTek Instruments, Winooski, VT, USA) at a wavelength of 450 nm and a reference wavelength of approximately 690 nm.

Telomere length

DNA was extracted from cells and tissues using a High Pure PCR Template Preparation Kit (Roche Boehringer-Mannheim, Grenzach-Wyhlen, Germany). Telomere length analysis was performed using a nonradioactive TeloTAGGG telomere length assay (Roche Boehringer-Mannheim), as described by the manufacturer. Briefly, 2–4 µg of DNA from each sample was digested using Hinf I/RsaI enzyme mix and separated via gel electrophoresis. DNA fragments were transferred to a nylon membrane (GE Healthcare, Little Chalfont, UK) by Southern transfer and hybridised to a digoxigenin (DIG)-labelled probe specific for telomeric repeats. The membrane was incubated with a DIG-specific antibody conjugated to alkaline phosphatase, and the probe was visualised by chemiluminescence detection using an image analyser (ImageQuant LAS 4000, GE Healthcare). The mean telomeric repeat binding factor lengths were compared with those of the molecular weight standard.

mRNA sequencing analysis

RNA sequencing of the hippocampal tissues from 3xTg-AD mice were performed by E-Biogen (Seoul, Korea).

RNA isolation

Total RNA from the hippocampal tissues of 3xTg-AD mice was isolated using the TRIzol reagent (Invitrogen). RNA quality was assessed on an Agilent 2100 bio-analyzer using the RNA 6000 Nano Chip (Agilent Technologies, Amstelveen, The Netherlands), and RNA quantification was performed using an ND-2000 spectrophotometer (Thermo Fisher Scientific).

Library preparation and sequencing

Libraries were prepared using 2 µg of total RNA using a SMARTer Stranded RNA-Seq Kit (Clontech Laboratories, Inc., Redwood City, CA, USA). mRNA enrichment was performed using a Poly(A) RNA Selection Kit (Lexogen, Inc., Vienna, Austria). The isolated mRNA was used for cDNA synthesis and shearing following the manufacturer's instructions. Indexing was performed using Illumina indexes 1–12. The enrichment step was carried out using polymerase chain reaction (PCR). Subsequently, the libraries were checked using an Agilent 2100 bioanalyzer and DNA High Sensitivity Ki t (5067-4626, Agilent Technologies,

Inc., Santa Clara, CA, USA) to evaluate the mean fragment size. Quantification was performed using the library quantification kit for the StepOne Real-Time PCR System (Life Technologies, Inc., Carlsbad, CA, USA). High-throughput sequencing was performed as sequencing of paired-end 100 base pairs using a HiSeq 2500 (Illumina, Inc., San Diego, CA, USA).

Data analysis

mRNA-Seq reads were mapped using the TopHat software tool to obtain the alignment file [52]. Differentially expressed genes (DEGs) were determined based on counts from unique and multiple alignments using coverage in BEDTools [53]. The read count data were processed based on the quantile normalization method using an Edge R in R (R Development Core Team) and Bioconductor [54]. The alignment files were also used to assemble transcripts, estimate their abundance, and detect the differential expression of genes or isoforms using Cufflinks (http://cole-trapnell-lab.github.io/cufflinks/). We used the fragments per kilobase of exon per million fragments method to determine the expression levels of the gene regions. Gene classification was based on searches performed in the Database for Annotation, Visualization and Integrated Discovery (DAVID, https://david.ncifcrf.gov/), which is designed to provide tools for the functional interpretation of large lists of genes/proteins [55, 56].

Gene ontology (GO) and signature analyses

GO analysis was conducted using DAVID bioinformatics resources [55]. The top 256 upregulated and down-regulated DEGs were used for enrichment analysis using DAVID and the Cytoscape plug-ins ClueGO and CluePedia. The criteria to select significant DEGs for these analyses were folding change >3, normalised data ($\log_2$) >4, and P-value < 0.05. We used the ClueGO v2.5.8 app of Cytoscape v3.8.2 with global network specificity to visualise the significant functional enrichment results of our study [57]. Using ClueGO analysis, we identified upregulated and down-regulated mRNAs, which were confirmed via RNA-Seq, in 3xTg-AD mice treated with GV1001 compared to those of 3xTg-AD mice treated with saline. Only the most significant term per group is labelled, and the colours represent the functional groups to which they belong. The size of the node represents the significance of enrichment. The functionally related groups partially overlapped.

Proteomics

Protein sample preparation

Cells were washed twice with ice-cold PBS and sonicated for 10 s with a Sonoplus homogeniser (Bandelin Electronics, Berlin, Germany) in a sample lysis solution composed of 7 M urea and 2 M thiourea,

4% 3-([3-cholamidopropyl] dimethylammonio)-1-propanesulphonate, 1% (w/v) DTT, 2% (v/v) Pharmalyte, and 1 mM benzamidine. The proteins were extracted for 1 h at 27° C using a vortex mixer. After centrifugation at 12,000 rpm for 1 h at 15° C, the insoluble material was discarded, and the soluble fraction was used for 2D gel electrophoresis. Protein concentrations were determined using the Bradford method.

2D PAGE

Immobilised pH gradient (IPG) dry strips (4-10 NL IPG, 13 cm, GE Healthcare) were reswelled for 9.5 h with Destreak rehydration solution and 0.5% IPG buffer and loaded with 150 µg of the sample. Isoelectric focusing (IEF) was performed at 20° C using an Ettan IPGphor 3 instrument (GE Healthcare, UK) following the manufacturer's instructions. For the IEF, the voltage was linearly increased at 100–8,000 V over 7 h for sample entry and then maintained at 8,000 V. The focus was complete after 55 kVh. Before running the second dimension, the strips were incubated for 15 min in equilibration buffer (75 mM Tris-Cl, pH 8.8, containing 6 M urea, 2% SDS, 0.002% bromophenol blue stock solution, and 29.3% glycerol), first with 1% DTT and then with 2.5% iodoacetamide. Equilibrated strips were inserted into SDS-PAGE gels (13 × 18 cm, 12%). SDS-PAGE was performed using an SE600 2D system (GE Healthcare, UK) following the manufacturer's instructions. The 2D gels were run at 20° C for 1,700 Vh.

Image analysis

Quantitative analysis of digitised images was performed using ImageMasterTM 2D Platinum 7.0 software (GE Healthcare, UK) according to the protocols provided by the manufacturer. The intensity of each spot was normalised to the total valid spot intensity. The selected protein spots showed a difference in protein expression of at least two-fold compared with the control or normal samples.

Peptide mass fingerprinting (PMF)

For protein identification with PMF, protein spots were excised, digested with trypsin (Promega, Madison, WI, USA), mixed with α cyano-4-hydroxycinnamic acid in 50% acetonitrile/0.1% trifluoroacetic acid (TFA), and subjected to matrix-assisted laser desorption ionisation-time of flight analysis (Microflex LRF 20, Bruker Daltonics, Billerica, MA, USA), as described by Fernandez et al. [58]. Spectra were collected from 300 shots per spectrum over the mass-to-charge (m/z) range of 600–3000 and calibrated by two-point internal calibration using trypsin autodigestion peaks (m/z 842.5099 and 2211.1046). The peak list was generated using Flex Analysis 3.0 (Bruker Daltonik GmbH, Bremen, Germany). The threshold used for peak selection was as follows: 500 for the minimum reso-

lution of monoisotopic mass and 5 for single-to-noise (S/N). The search programme MASCOT, developed by Matrix Science (http://www.matrixscience.com/) [59], was used for protein identification using PMF. The following parameters were used for the database search: trypsin as the cleaving enzyme, a maximum of one missed cleavage, iodoacetamide (Cys) as a complete modification, oxidation (Met) as a partial modification, monoisotopic mass, and mass tolerance of ± 0.1 Da. The PMF acceptance criteria were based on probability scoring.

Statistical analysis

All data are presented as mean ± standard deviation (SD) of five or more independent experiments. Statistical analyses of three or more datasets were performed using one-way analysis of variance (ANOVA), followed by Tukey's post-hoc comparisons. Student's *t*-test was used for comparison between the two groups. The survival outcomes were assessed using the Kaplan-Meier method and compared using log-rank tests. P-values <0.05 were considered statistically significant, and statistical analyses were performed with SPSS 21.0 (SPSS Inc., Chicago, IL, USA).

Data and materials availability

The data and materials that support the findings of current study are available from the corresponding author upon reasonable request.

AUTHOR CONTRIBUTIONS

Park HH, Kwon HS, Lee KY, Kim SJ and Koh.SH made substantial contributions to the conception and design of the work. Park HH, Kwon HS, and Lee KY interpreted the data and drafted the manuscript. Koh SH and Kim SJ revised the manuscript. Park HH, Kim YE and Choi NY made substantial contributions to analysis and investigation of data. Park HH, Kim YE, Son JW and Choi NY performed experiments. Lee KY, Han MH, Park DW, Kim SJ and Koh SH supervised the study. Park HH, Kwon HS, and Lee KY contributed equally to the study. All authors have read and approved the final manuscript.

CONFLICTS OF INTEREST

ETHICAL STATEMENT

All experiments involving animals were conducted in compliance with the Hanyang University guidelines for the care and use of laboratory animals. Our study was approved by the Institutional Animal Care and Use Committee of Hanyang University (2014-0051A).

FUNDING

REFERENCES

1. Ganguli M, Dodge HH, Shen C, Pandav RS, DeKosky ST. Alzheimer disease and mortality: a 15-year epidemiological study. Arch Neurol. 2005; 62:779–84.
https://doi.org/10.1001/archneur.62.5.779
PMID:15883266

2. Campbell-Taylor I. Contribution of Alzheimer disease to mortality in the United States. Neurology. 2014; 83:1302.
https://doi.org/10.1212/01.wnl.0000455099.43083.c6
PMID:25267987

3. GBD 2016 Dementia Collaborators. Global, regional, and national burden of Alzheimer's disease and other dementias, 1990-2016: a systematic analysis for the Global Burden of Disease Study 2016. Lancet Neurol. 2019; 18:88–106.
https://doi.org/10.1016/S1474-4422(18)30403-4
PMID:30497964

4. Sevigny J, Chiao P, Bussière T, Weinreb PH, Williams L, Maier M, Dunstan R, Salloway S, Chen T, Ling Y, O'Gorman J, Qian F, Arastu M, et al. The antibody aducanumab reduces Aβ plaques in Alzheimer's disease. Nature. 2016; 537:50–6.
https://doi.org/10.1038/nature19323
PMID:27582220

5. Panza F, Seripa D, Lozupone M, Solfrizzi V, Imbimbo BP, Barulli MR, Tortelli R, Capozzo R, Bisceglia P, Dimitri A, Stallone R, Dibello V, Quaranta N, et al. The potential of solanezumab and gantenerumab to prevent Alzheimer's disease in people with inherited mutations that cause its early onset. Expert Opin Biol Ther. 2018; 18:25–35.
https://doi.org/10.1080/14712598.2018.1389885
PMID:29037101

6. Xia X, Jiang Q, McDermott J, Han JJ. Aging and Alzheimer's disease: Comparison and associations

from molecular to system level. Aging Cell. 2018; 17:e12802.
https://doi.org/10.1111/acel.12802
PMID:29963744

7. Azam S, Haque ME, Balakrishnan R, Kim IS, Choi DK. The Ageing Brain: Molecular and Cellular Basis of Neurodegeneration. Front Cell Dev Biol. 2021; 9:683459.
https://doi.org/10.3389/fcell.2021.683459
PMID:34485280

8. Hou Y, Dan X, Babbar M, Wei Y, Hasselbalch SG, Croteau DL, Bohr VA. Ageing as a risk factor for neurodegenerative disease. Nat Rev Neurol. 2019; 15:565–81.
https://doi.org/10.1038/s41582-019-0244-7
PMID:31501588

9. Castelli V, Benedetti E, Antonosante A, Catanesi M, Pitari G, Ippoliti R, Cimini A, d'Angelo M. Neuronal Cells Rearrangement During Aging and Neurodegenerative Disease: Metabolism, Oxidative Stress and Organelles Dynamic. Front Mol Neurosci. 2019; 12:132.
https://doi.org/10.3389/fnmol.2019.00132
PMID:31191244

10. Fukumoto H, Rosene DL, Moss MB, Raju S, Hyman BT, Irizarry MC. Beta-secretase activity increases with aging in human, monkey, and mouse brain. Am J Pathol. 2004; 164:719–25.
https://doi.org/10.1016/s0002-9440(10)63159-8
PMID:14742275

11. Kern A, Roempp B, Prager K, Walter J, Behl C. Down-regulation of endogenous amyloid precursor protein processing due to cellular aging. J Biol Chem. 2006; 281:2405–13.
https://doi.org/10.1074/jbc.M505625200
PMID:16303768

12. Koh SH, Choi SH, Jeong JH, Jang JW, Park KW, Kim EJ, Kim HJ, Hong JY, Yoon SJ, Yoon B, Kang JH, Lee JM, Park HH, et al. Telomere shortening reflecting physical aging is associated with cognitive decline and dementia conversion in mild cognitive impairment due to Alzheimer's disease. Aging (Albany NY). 2020; 12:4407–23.
https://doi.org/10.18632/aging.102893
PMID:32126022

13. Forero DA, González-Giraldo Y, López-Quintero C, Castro-Vega LJ, Barreto GE, Perry G. Meta-analysis of Telomere Length in Alzheimer's Disease. J Gerontol A Biol Sci Med Sci. 2016; 71:1069–73.
https://doi.org/10.1093/gerona/glw053
PMID:27091133

14. Park HH, Yu HJ, Kim S, Kim G, Choi NY, Lee EH, Lee YJ, Yoon MY, Lee KY, Koh SH. Neural stem cells injured by

oxidative stress can be rejuvenated by GV1001, a novel peptide, through scavenging free radicals and enhancing survival signals. Neurotoxicology. 2016; 55:131–41.
https://doi.org/10.1016/j.neuro.2016.05.022
PMID:27265016

15. Park HH, Lee KY, Kim S, Lee JW, Choi NY, Lee EH, Lee YJ, Lee SH, Koh SH. Novel vaccine peptide GV1001 effectively blocks β-amyloid toxicity by mimicking the extra-telomeric functions of human telomerase reverse transcriptase. Neurobiol Aging. 2014; 35:1255–74.
https://doi.org/10.1016/j.neurobiolaging.2013.12.015
PMID:24439482

16. Kwon HS, Kim YE, Park HH, Son JW, Choi H, Lee YJ, Kim HY, Lee KY, Koh SH. Neuroprotective Effects of GV1001 in Animal Stroke Model and Neural Cells Subject to Oxygen-Glucose Deprivation/Reperfusion Injury. J Stroke. 2021; 23:420–36.
https://doi.org/10.5853/jos.2021.00626
PMID:34649386

17. Koh SH, Kwon HS, Choi SH, Jeong JH, Na HR, Lee CN, Yang Y, Lee AY, Lee JH, Park KW, Han HJ, Kim BC, Park JS, et al. Efficacy and safety of GV1001 in patients with moderate-to-severe Alzheimer's disease already receiving donepezil: a phase 2 randomized, double-blind, placebo-controlled, multicenter clinical trial. Alzheimers Res Ther. 2021; 13:66.
https://doi.org/10.1186/s13195-021-00803-w
PMID:33771205

18. Park HH, Lee KY, Park DW, Choi NY, Lee YJ, Son JW, Kim S, Moon C, Kim HW, Rhyu IJ, Koh SH. Tracking and protection of transplanted stem cells using a ferrocenecarboxylic acid-conjugated peptide that mimics hTERT. Biomaterials. 2018; 155:80–91.
https://doi.org/10.1016/j.biomaterials.2017.11.009
PMID:29169040

19. Ullman-Culleré MH, Foltz CJ. Body condition scoring: a rapid and accurate method for assessing health status in mice. Lab Anim Sci. 1999; 49:319–23.
PMID:10403450

20. Lourenço AB, Artal-Sanz M. The Mitochondrial Prohibitin (PHB) Complex in C. elegans Metabolism and Ageing Regulation. Metabolites. 2021; 11:636.
https://doi.org/10.3390/metabo11090636
PMID:34564452

21. Merkwirth C, Martinelli P, Korwitz A, Morbin M, Brönneke HS, Jordan SD, Rugarli EI, Langer T. Loss of prohibitin membrane scaffolds impairs mitochondrial architecture and leads to tau hyperphosphorylation and neurodegeneration. PLoS Genet. 2012; 8:e1003021.
https://doi.org/10.1371/journal.pgen.1003021

PMID:23144624

22. Imperlini E, Orrù S, Corbo C, Daniele A, Salvatore F. Altered brain protein expression profiles are associated with molecular neurological dysfunction in the PKU mouse model. J Neurochem. 2014; 129:1002–12.
https://doi.org/10.1111/jnc.12683
PMID:24548049

23. Zhao Y, Wu Y, Hu H, Cai J, Ning M, Ni X, Zhong C. Downregulation of transketolase activity is related to inhibition of hippocampal progenitor cell proliferation induced by thiamine deficiency. Biomed Res Int. 2014; 2014:572915.
https://doi.org/10.1155/2014/572915 PMID:25028661

24. Zhang Z, Deng X, Liu Y, Liu Y, Sun L, Chen F. PKM2, function and expression and regulation. Cell Biosci. 2019; 9:59.
https://doi.org/10.1186/s13578-019-0317-8
PMID:31391918

25. Cai Y, Zhu HX, Li JM, Luo XG, Patrylo PR, Rose GM, Streeter J, Hayes R, Wang KK, Yan XX, Jeromin A. Age-related intraneuronal elevation of αII-spectrin breakdown product SBDP120 in rodent forebrain accelerates in 3×Tg-AD mice. PLoS One. 2012; 7:e37599.
https://doi.org/10.1371/journal.pone.0037599
PMID:22723836

26. Xu M, He D, Teng H, Chen L, Song H, Huang Q. Physiological and proteomic analyses of coix seed aging during storage. Food Chem. 2018; 260:82–9.
https://doi.org/10.1016/j.foodchem.2018.03.129
PMID:29699686

27. Lee BY, Han JA, Im JS, Morrone A, Johung K, Goodwin EC, Kleijer WJ, DiMaio D, Hwang ES. Senescence-associated beta-galactosidase is lysosomal beta-galactosidase. Aging Cell. 2006; 5:187–95.
https://doi.org/10.1111/j.1474-9726.2006.00199.x
PMID:16626397

28. Blackburn EH. Telomere states and cell fates. Nature. 2000; 408:53–6.
https://doi.org/10.1038/35040500
PMID:11081503

29. von Zglinicki T, Martin-Ruiz CM. Telomeres as biomarkers for ageing and age-related diseases. Curr Mol Med. 2005; 5:197–203.
https://doi.org/10.2174/1566524053586545
PMID:15974873

30. Kalanj-Bognar S, Rundek T, Furac I, Demarin V, Cosović C. Leukocyte lysosomal enzymes in Alzheimer's disease and Down's syndrome. J Gerontol A Biol Sci Med Sci. 2002; 57:B16–21.
https://doi.org/10.1093/gerona/57.1.b16
PMID:11773202

31. Wolkowitz OM, Mellon SH, Epel ES, Lin J, Dhabhar FS, Su Y, Reus VI, Rosser R, Burke HM, Kupferman E, Compagnone M, Nelson JC, Blackburn EH. Leukocyte telomere length in major depression: correlations with chronicity, inflammation and oxidative stress--preliminary findings. PLoS One. 2011; 6:e17837.
https://doi.org/10.1371/journal.pone.0017837
PMID:21448457

32. Yu GL, Bradley JD, Attardi LD, Blackburn EH. *In vivo* alteration of telomere sequences and senescence caused by mutated Tetrahymena telomerase RNAs. Nature. 1990; 344:126–32.
https://doi.org/10.1038/344126a0 PMID:1689810

33. Lulkiewicz M, Bajsert J, Kopczynski P, Barczak W, Rubis B. Telomere length: how the length makes a difference. Mol Biol Rep. 2020; 47:7181–8.
https://doi.org/10.1007/s11033-020-05551-y
PMID:32876842

34. Blasco MA. Telomere length, stem cells and aging. Nat Chem Biol. 2007; 3:640–9.
https://doi.org/10.1038/nchembio.2007.38
PMID:17876321

35. Galasko D, Montine TJ. Biomarkers of oxidative damage and inflammation in Alzheimer's disease. Biomark Med. 2010; 4:27–36.
https://doi.org/10.2217/bmm.09.89 PMID:20383271

36. Wang Q, Zhan Y, Pedersen NL, Fang F, Hägg S. Telomere Length and All-Cause Mortality: A Meta-analysis. Ageing Res Rev. 2018; 48:11–20.
https://doi.org/10.1016/j.arr.2018.09.002
PMID:30254001

37. Yarian CS, Toroser D, Sohal RS. Aconitase is the main functional target of aging in the citric acid cycle of kidney mitochondria from mice. Mech Ageing Dev. 2006; 127:79–84.
https://doi.org/10.1016/j.mad.2005.09.028
PMID:16289253

38. Tan CC, Yu JT, Wang HF, Tan MS, Meng XF, Wang C, Jiang T, Zhu XC, Tan L. Efficacy and safety of donepezil, galantamine, rivastigmine, and memantine for the treatment of Alzheimer's disease: a systematic review and meta-analysis. J Alzheimers Dis. 2014; 41:615–31.
https://doi.org/10.3233/JAD-132690
PMID:24662102

39. Baruch-Eliyahu N, Rud V, Braiman A, Priel E. Telomerase increasing compound protects hippocampal neurons from amyloid beta toxicity by enhancing the expression of neurotrophins and plasticity related genes. Sci Rep. 2019; 9:18118.
https://doi.org/10.1038/s41598-019-54741-7
PMID:31792359

40. Ko YJ, Kwon KY, Kum KY, Lee WC, Baek SH, Kang MK,

Shon WJ. The Anti-Inflammatory Effect of Human Telomerase-Derived Peptide on P. gingivalis Lipopolysaccharide-Induced Inflammatory Cytokine Production and Its Mechanism in Human Dental Pulp Cells. Mediators Inflamm. 2015; 2015:385127. https://doi.org/10.1155/2015/385127 PMID:26604431

41. Saretzki G. Extra-telomeric functions of human telomerase: cancer, mitochondria and oxidative stress. Curr Pharm Des. 2014; 20:6386–403. https://doi.org/10.2174/1381612820666140630095606 PMID:24975608

42. Chung HK, Cheong C, Song J, Lee HW. Extratelomeric functions of telomerase. Curr Mol Med. 2005; 5:233–41. https://doi.org/10.2174/1566524053586635 PMID:15974878

43. Martínez P, Blasco MA. Telomeric and extra-telomeric roles for telomerase and the telomere-binding proteins. Nat Rev Cancer. 2011; 11:161–76. https://doi.org/10.1038/nrc3025 PMID:21346783

44. Ding X, Liu X, Wang F, Wang F, Geng X. Role of Senescence and Neuroprotective Effects of Telomerase in Neurodegenerative Diseases. Rejuvenation Res. 2020; 23:150–8. https://doi.org/10.1089/rej.2018.2115 PMID:31170886

45. Park H, Kwon HS, Lee KY, Kim YE, Son JW, Choi NY, Lee EJ, Han MH, Park DW, Kim S, Koh SH. GV1001 modulates neuroinflammation and improves memory and behavior through the activation of gonadotropin-releasing hormone receptors in a triple transgenic Alzheimer's disease mouse model. Brain Behav Immun. 2024; 115:295–307. https://doi.org/10.1016/j.bbi.2023.10.021 PMID:37884161

46. LaFerla FM, Green KN. Animal models of Alzheimer disease. Cold Spring Harb Perspect Med. 2012; 2:a006320. https://doi.org/10.1101/cshperspect.a006320 PMID:23002015

47. Olfert E, Bhasin J, Latt R, Macallum E, McCutcheon K, Rainnie D, Schunk M. The CCAC guidelines on: choosing an appropriate endpoint in experiments using animals for research, teaching and testing Canadian Council on Animal Care guideline. 1998; 1:1–30.

48. Studer L, Tabar V, McKay RD. Transplantation of expanded mesencephalic precursors leads to recovery in parkinsonian rats. Nat Neurosci. 1998; 1:290–5. https://doi.org/10.1038/1105 PMID:10195162

49. Chojnacki A, Weiss S. Production of neurons, astrocytes and oligodendrocytes from mammalian CNS stem cells. Nat Protoc. 2008; 3:935–40. https://doi.org/10.1038/nprot.2008.55 PMID:18536641

50. Currle DS, Hu JS, Kolski-Andreaco A, Monuki ES. Culture of mouse neural stem cell precursors. J Vis Exp. 2007; 2:152. https://doi.org/10.3791/152 PMID:18830426

51. Choi YK, Maki T, Mandeville ET, Koh SH, Hayakawa K, Arai K, Kim YM, Whalen MJ, Xing C, Wang X, Kim KW, Lo EH. Dual effects of carbon monoxide on pericytes and neurogenesis in traumatic brain injury. Nat Med. 2016; 22:1335–41. https://doi.org/10.1038/nm.4188 PMID:27668935

52. Trapnell C, Pachter L, Salzberg SL. TopHat: discovering splice junctions with RNA-Seq. Bioinformatics. 2009; 25:1105–11. https://doi.org/10.1093/bioinformatics/btp120 PMID:19289445

53. Quinlan AR, Hall IM. BEDTools: a flexible suite of utilities for comparing genomic features. Bioinformatics. 2010; 26:841–2. https://doi.org/10.1093/bioinformatics/btq033 PMID:20110278

54. Gentleman RC, Carey VJ, Bates DM, Bolstad B, Dettling M, Dudoit S, Ellis B, Gautier L, Ge Y, Gentry J, Hornik K, Hothorn T, Huber W, et al. Bioconductor: open software development for computational biology and bioinformatics. Genome Biol. 2004; 5:R80. https://doi.org/10.1186/gb-2004-5-10-r80 PMID:15461798

55. Huang da W, Sherman BT, Lempicki RA. Systematic and integrative analysis of large gene lists using DAVID bioinformatics resources. Nat Protoc. 2009; 4:44–57. https://doi.org/10.1038/nprot.2008.211 PMID:19131956

56. Huang da W, Sherman BT, Lempicki RA. Bioinformatics enrichment tools: paths toward the comprehensive functional analysis of large gene lists. Nucleic Acids Res. 2009; 37:1–13. https://doi.org/10.1093/nar/gkn923 PMID:19033363

57. Bindea G, Mlecnik B, Hackl H, Charoentong P, Tosolini M, Kirilovsky A, Fridman WH, Pagès F, Trajanoski Z, Galon J. ClueGO: a Cytoscape plug-in to decipher functionally grouped gene ontology and pathway annotation networks. Bioinformatics. 2009; 25:1091–3. https://doi.org/10.1093/bioinformatics/btp101 PMID:19237447

58. Fernandez J, Gharahdaghi F, Mische SM. Routine identification of proteins from sodium dodecyl sulfate-polyacrylamide gel electrophoresis (SDS-PAGE) gels or polyvinyl difluoride membranes using matrix assisted laser desorption/ionization-time of flight-mass spectrometry (MALDI-TOF-MS). Electrophoresis. 1998; 19:1036–45.
https://doi.org/10.1002/elps.1150190619
PMID:9638950

59. Cottrell JS. Protein identification using MS/MS data. J Proteomics. 2011; 74:1842–51.
https://doi.org/10.1016/j.jprot.2011.05.014
PMID:21635977
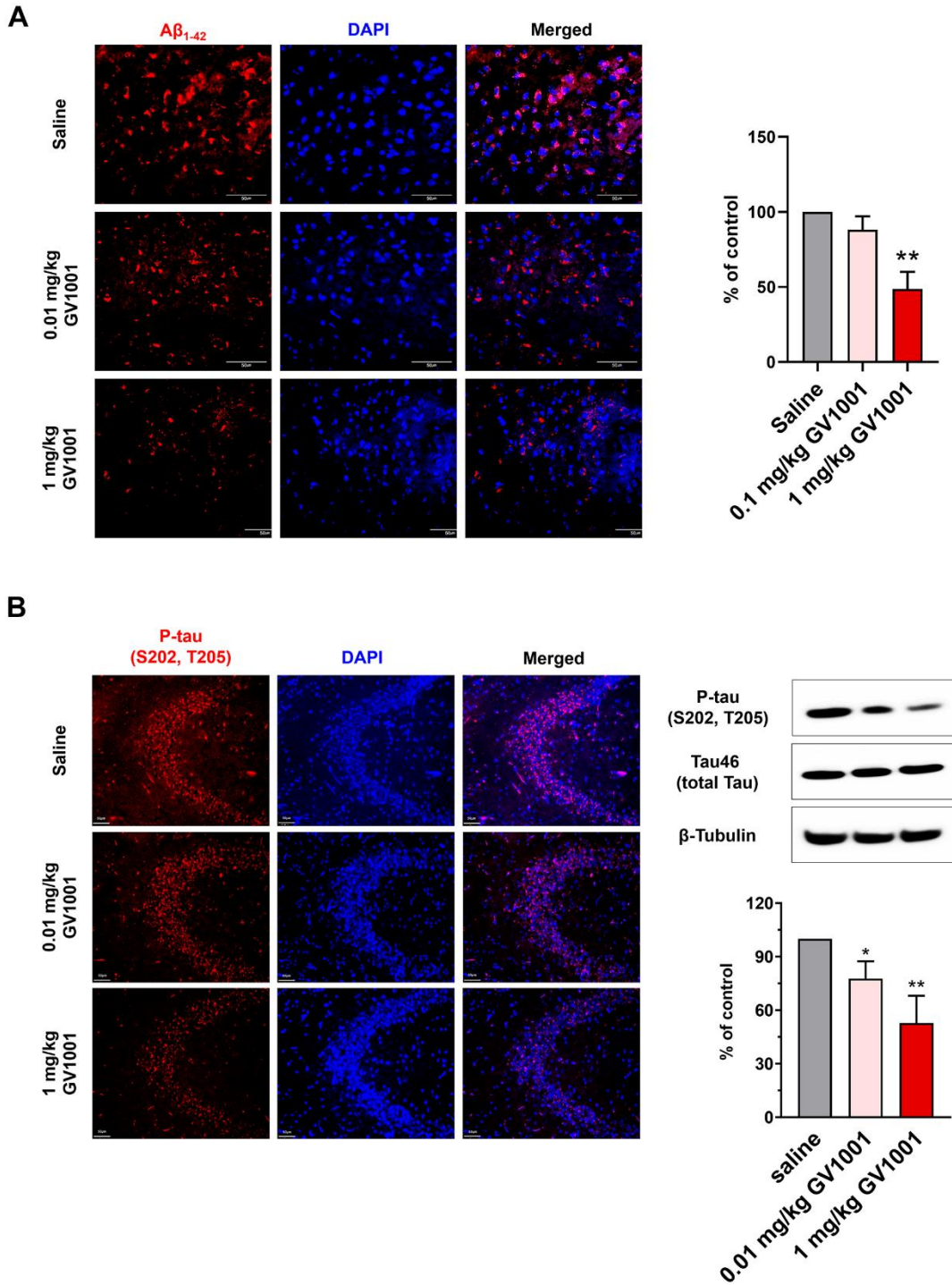
Supplementary Figure 1. Effect of GV1001 on amyloid beta (Aβ)$_{1-42}$ and p-tau in the brain of 3xTg AD mice in a dose-dependent manner. To evaluate the dose responsiveness of GV1001, we injected 0.01 mg/kg and 1 mg/kg GV1001 into middle-aged 3xTg AD mice subcutaneously for two months, from 12 months to 14 months of age. The results showed that 1 mg/kg GV1001 had a stronger effect against Aβ$_{1-42}$ (**A**) and p-tau (**B**) in the brains of middle-aged 3xTg mice than 0.01 mg/kg.
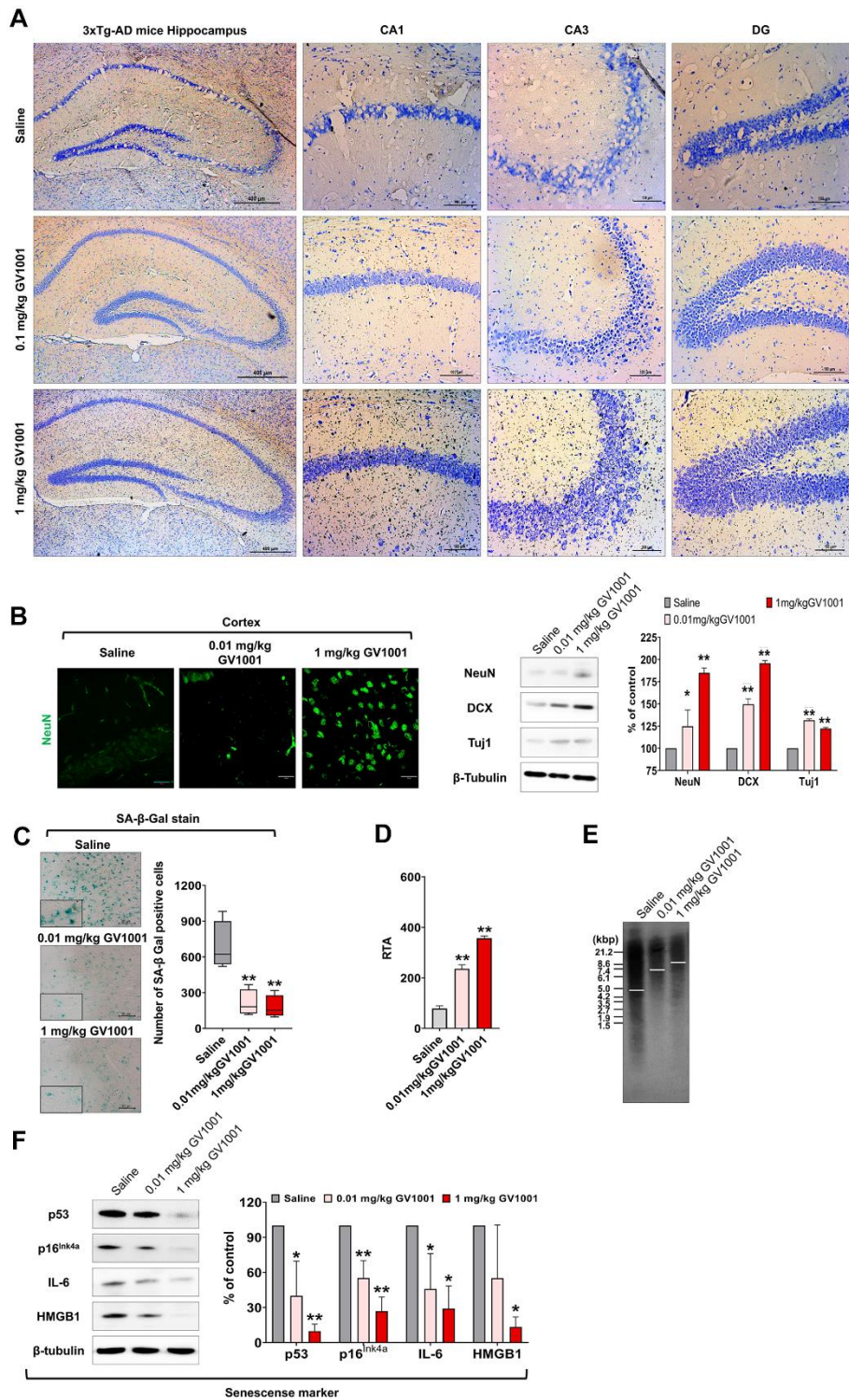
Supplementary Figure 2. GV1001 has a strong effect on senescence in the brain of 3xTg AD mice in a dose-dependent manner. Injection of 1 mg/kg GV1001 showed stronger effect than 0.01 mg/kg against neurodegeneration (**A**, **B**), and senescence (**C**–**F**) in the brains of middle-aged 3xTg AD mice. Therefore, we used 1 mg/kg GV1001 in the main study.

Supplementary Tables

Supplementary Table 1. Criteria for an appropriate endpoint.

Variable	Score
Weight change	
0 normal	
1 <10% Weight loss	
2 10~15% Weight loss	
3 >20% Weight loss	
Body Condition Scoring, BCS (Extended Table. 2)	
0 BCS >3	
1 BCS >2 and <3	
2 BCS >1 and <2	
3 BCS 1 or less	
Appearance	
0 normal	
1 lack of hair trim	
2 Rough hair, nose / eye discharge	
3 Severely rough hair, abnormal posture, dilated pupil	
Clinical symptoms	
0 normal	
1 Slight change	
2 1~2° C Body temperature change, heart rate and respiratory rate ~ 30% increase	
3 Changes in body temperature over 2° C, heart rate and respiratory rate ~ 50% increase or decrease abruptly.	
behavior	
0 normal	
1 Slight change	
2 Abnormal, decreased motion, decreased awareness, inactive	
3 Crying cry, self-cutting, hardly moving	
Response to external reaction	
0 normal	
1 Mild depression / increased reaction	
2 Severe abnormal reactions.	
3 Aggressive reaction or coma.	
Total	

Various items were used to evaluate the condition of old 3xTg AD mice, as shown in Supplementary Table 1 [Establishing Humane Endpoints - Office of Research Ethics (https://www.compliance.iastate.edu.policies.docs)]. A total score of >5 or a score of 3 for any variable was determined, regardless of the total score for humane euthanasia.

Supplementary Table 2. Body condition score.

Mouse

BC1

Haggard / Weakness
- The skeleton protrudes prominently. Almost no flesh.

BC2

Bad management
- The separation of the protruding vertebra was observed.
- Pelvic bones of the dorsal can be easily palpated.

BC3

Proper management
- The spinal and pelvic bones are not noticeable, and can be palpable with slight pressure.

BC4

Excessive management
- Dorsal bones are not segmented but are continuously observed.
- The vertebrae must be reliably pressurized.

BC5

obesity
- The mouse seems to be flat and bulging.
- The skeleton has disappeared because the skin and subcutaneous fat are thick.

A body condition score (BCS) is used to evaluate fat and muscle development in livestock. Scoring techniques for mice are widely used to assess their health and fitness. BCS is an easy and objective assessment method that can be incorporated into humane endpoints. BCS can provide a more accurate estimate of health and fitness than body weight measurements, and it is useful in chronic studies in which animals lose muscle mass and fat over time.